ACS OMEGA

Open Access

http://pubs.acs.org/journal/acsodf

Article

Enhanced Antibacterial Activity against *Escherichia coli* Based on Cationic Carbon Dots Assembling with 5-Aminolevulinic Acid

Jingfang Shangguan,* Zhenjing Wu, Chengjie Qiao, Yuyang Zhang, Lin Li, Qilu Li, Yiqiao Gao, Huijuan Yan, and Wei Liu*

Cite This: *ACS Omega* 2024, 9, 7034−7042

Read Online

ACCESS | Metrics & More | Article Recommendations | Supporting Information

ABSTRACT: Carbon dots (CDs) with positive surface charges are considered one of the encouraging nanomedications for antibacterial applications. However, due to the distinctive membrane structure of Gram-negative bacteria, cationic CDs with relatively high concentrations are usually required for effective treatment, which might bring out serious safety issues at high doses. Therefore, it is of substantial significance to improve the killing efficiency of cationic CDs on Gram-negative bacteria at appropriately low concentrations. In this work, optimized cationic CDs ($bPEI_{25\,000}$-CDs) were prepared via a hydrothermal method with citric acid and branched PEI_{25000}, which offered a positive surface potential, elimination abilities against *Escherichia coli*, and relatively high biosafety. The optimized $bPEI_{25\,000}$-CDs can further assemble with the clinical photodynamic therapy (PDT) drug 5-aminolevulinic acid (5-ALA) through electrostatic interaction. Moreover, compared with $bPEI_{25\,000}$-CDs and 5-ALA, the bacterial survival rate was significantly reduced by the ALA-$bPEI_{25\,000}$-CD-induced PDT effect. Even when the dose of $bPEI_{25\,000}$-CD carrier was halved, the bacterial survival could be reduced by 44.4% after light exposure compared to those incubated in the dark. The investigation of the bacterial morphology, membrane potential, and intracellular ROS production suggested that the enhanced antibacterial activity may be due to the membrane dysfunction and cell damage resulting from the high interaction between positively charged ALA-$bPEI_{25\,000}$-CDs and the bacterial cell membrane. Meanwhile, the cationic ALA-$bPEI_{25\,000}$-CDs may facilitate the cellular uptake of 5-ALA, resulting in a more efficient PDT effect. In summary, the antibacterial strategy proposed in this study will provide a novel approach for expanding the application of CD-based nanomedications.

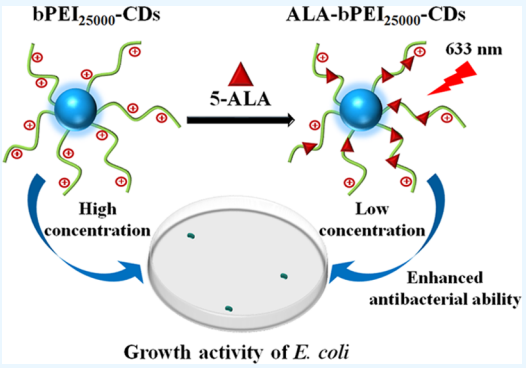

1. INTRODUCTION

Bacterial infections have become one of the most serious threats to human health, food safety, and medical development. Antibiotics are commonly used clinical drugs for bacterial infectious treatment, and the misuse and overuse of antibiotics have accelerated the evolution of bacterial resistance.[1] With the rapid development of nanoscience and nanotechnology, nanomaterial-based antimicrobial agents, such as nanosilver,[2,3] titanium dioxide,[4,5] graphene,[6,7] and cationic polymer nanoparticles,[8] have shown great potential in overcoming drug resistance by virtue of their unique characteristics. However, these nanosystems are still restricted to certain limits for practical applications. For instance, the potential toxicity risks caused by metal ion release and the relatively slow clearance of nanomedications with larger sizes *in vivo* should be clarified. Thus, novel nanomaterials with improved safety and effective antibacterial activity are strongly desired.[9,10]

Carbon dots (CDs) are carbon nanomaterials featured with high fluorescence stability, good biocompatibility, low toxicity, easy preparation, and wide applications, such as fluorescence imaging,[11−13] biochemical analysis,[14−16] photocatalysis,[17,18] and cancer therapy.[19,20] Recently, CD-based hypotoxic antimicrobial materials have drawn extensive attention from the scientific community. For instance, polyethylenimine (PEI), as a cationic polymer with many primary, secondary, and tertiary amino groups, has been popularly used in drug delivery, gene transfection, and antibacterial applications.[21−23] Due to the strong penetration and disruption ability of the positively charged PEI to bacterial cell membranes, the PEI-functionalized CDs provide candidates for the fabrication of antibacterial nanomedications.[24−26] However, despite very promising capabilities, some cationic CD-based antibacterial nanomedications in clinical treatment still face a critical issue that the higher concentrations are required to eliminate Gram-

Received: November 9, 2023
Revised: January 3, 2024
Accepted: January 15, 2024
Published: February 1, 2024

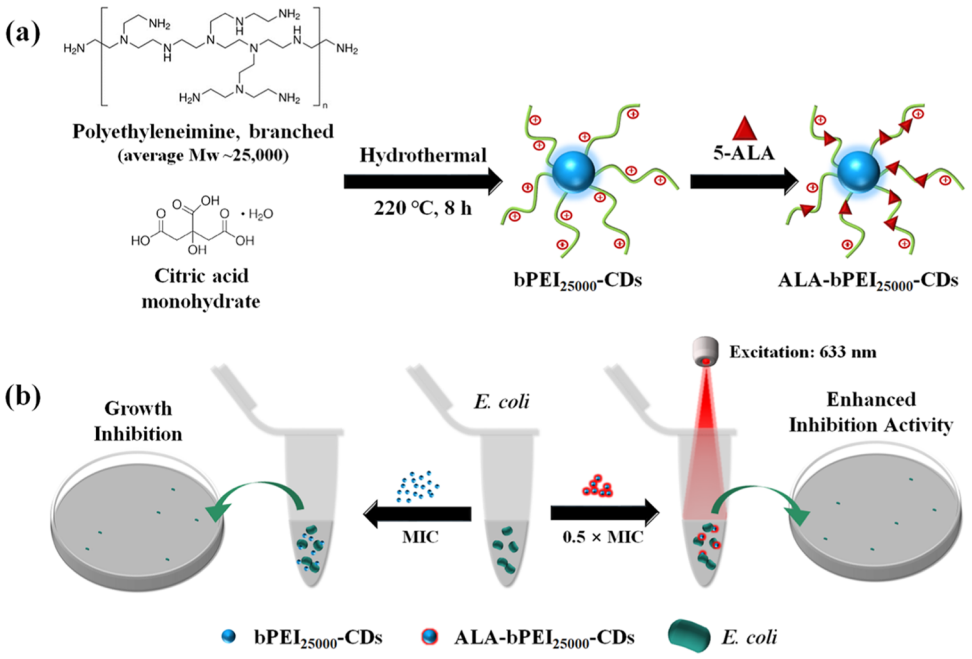

Figure 1. Schematic illustration of (a) the fabrication of bPEI$_{25\,000}$-CDs and ALA-bPEI$_{25\,000}$-CDs. (b) The inactivation performance of bPEI$_{25\,000}$-CDs and ALA-bPEI$_{25\,000}$-CDs on *E. coli* (MIC is the minimum inhibitory concentration of bPEI$_{25\,000}$-CDs against *E. coli*).

negative bacteria compared to that for Gram-positive bacteria, which accordingly address safety concerns.[27−29] Hence, constant efforts have been devoted to improving the antibacterial efficacy of cationic CD-based antibacterial nanomedications, particularly against Gram-negative bacteria.

5-Aminolevulinic acid (5-ALA), a hydrophilic clinical photodynamic therapy (PDT) drug approved by the U.S. Food and Drug Administration, has been commonly employed to treat dermatological disorders and cancer-related diseases by producing photoactive endogenous porphyrins through a series of enzymatic reactions and followed by converting the surrounding oxygen molecules into reactive oxygen species (ROS).[30−32] Compared to carbon dots, there are far fewer studies on the use of 5-ALA for bacterial elimination. It has been reported that Gram-negative bacteria are usually less sensitive to 5-ALA-induced PDT than Gram-positive bacteria due to differences in the cell membrane structures and the quantity, type, and distribution of endogenous porphyrins induced by 5-ALA from different strains.[33−37] Therefore, nanomedications taking advantage of the abilities of cationic CDs in disrupting cell membranes and 5-ALA for PDT have enormous potential to realize enhanced antibacterial efficiencies against Gram-negative bacteria, which is of vital significance for clinical applications. In this work, the optimized bPEI$_{25\,000}$-CDs were prepared by hydrothermal method using branched polyethylenimine (bPEI, average Mw 25000) and citric acid as the raw materials, which demonstrated positive surface charges, antibacterial ability, and good biocompatibility. A coassembly was further formed (ALA-bPEI$_{25\,000}$-CDs) by integrating bPEI$_{25\,000}$-CDs with 5-ALA via electrostatic interaction (Figure 1a). An enhanced inhibition effect on Gram-negative *Escherichia coli* (*E. coli*) was observed for ALA-bPEI$_{25\,000}$-CD treatment after photoexcitation compared to those for 5-ALA and bPEI$_{25\,000}$-CDs, respectively. Additionally, a relatively satisfactory elimination effect was obtained even after reducing the amount of bPEI$_{25\,000}$-CD carrier (Figure 1b). Hence, this research offers a new perspective on expanding novel nanoantimicrobials with low cost, simple preparation, and efficient bacterial inhibition activity.

2. EXPERIMENTAL SECTION

2.1. Materials. *E. coli* (CMCC44102) was purchased from the Shanghai Bioresource Collection Center. Human liver HL-7702 cells (L02), human skin fibroblast (HSF) cells, and human embryonic kidney epithelial cells (HEK-293T) were obtained from iCell Bioscience Inc. (Shanghai, China). Blood samples of Sprague-Dawley rats were obtained from the Laboratory Animal Center (Xinxiang Medical University, China), and the study protocol on the Ethics of Animal was approved by the Ethics Committee of Xinxiang Medical University. Citric acid monohydrate, branched polyethylenimine (bPEI$_{25\,000}$, average Mw 25 000 by LS), and 5-aminolevulinic acid hydrochloride (5-ALA) were provided by Sigma-Aldrich (St. Louis, MO). The cell counting kit-8 and fluorometric intracellular ROS kit were purchased from Shanghai BESTBIO Technical Co., Ltd. (Shanghai, China). Ultrapure water (18.2 MΩ, Millipore Co.) was used in all experiments. More detailed information on materials and instruments are listed in Text S1 and S2.

2.2. Irradiation Parameters. Irradiation was performed with a red diode laser (633 ± 3 fwhm nm) as the light source (Changchun New Industries Optoelectronics Technology Co., Ltd.). The photoexcitation was performed with a total specific dose of 177 J/cm^2 and different irradiation periods (10, 20, and 30 min). The laser probe was placed above the irradiated samples at a vertical distance of 5 cm.

2.3. Preparation of bPEI$_{25\,000}$-CDs. The optimized bPEI$_{25\,000}$-CDs were prepared via the one-pot hydrothermal method. Briefly, 0.7 g of citric acid monohydrate and 2.1 g of bPEI$_{25\,000}$ were sequentially dissolved in 15 mL of deionized water. Then, the resulting clear solution was transferred to a 50 mL hydrothermal reactor and heated at 220 °C for 8 h to produce bPEI$_{25\,000}$-CDs. The obtained bPEI$_{25\,000}$-CDs were

https://doi.org/10.1021/acsomega.3c08914
ACS Omega 2024, 9, 7034−7042

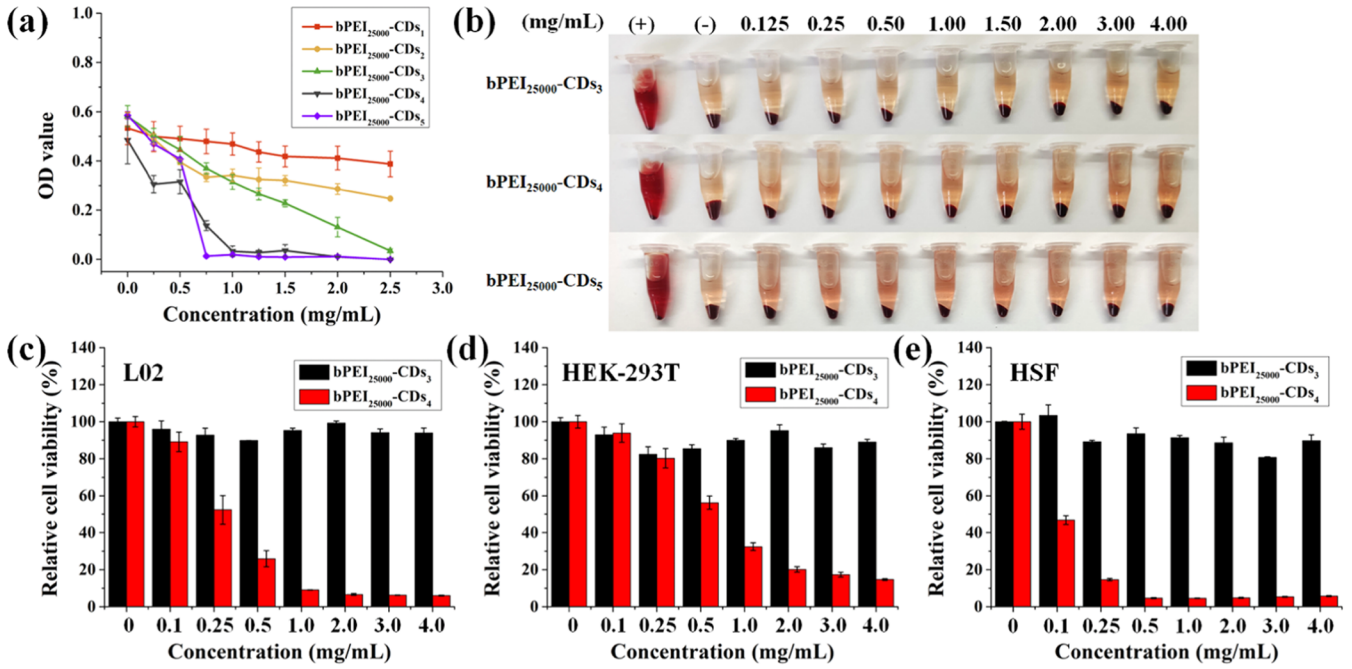

Figure 2. (a) Proliferation curves of different bPEI$_{25\,000}$-CDs against *E. coli*. (b) Hemostasis test of different bPEI$_{25\,000}$-CDs ((+) and (−) refer to deionized water and 0.9% normal saline, respectively). The cytotoxicity investigation of different bPEI$_{25\,000}$-CDs on L02 (c), HEK-293T (d), and HSF (e) cells.

first filtered through a 0.22 μm membrane and then purified using 20 kDa dialysis bags against ultrapure water for 48 h. CDs prepared without bPEI$_{25\,000}$ under the same conditions were defined as bare CDs. All samples were stored in a desiccator after freeze-drying.

2.4. Preparation of ALA-bPEI$_{25\,000}$-CDs. 5-ALA was loaded onto bPEI$_{25\,000}$-CDs by electrostatic adsorption and purified by dialysis. A standard curve was established to detect the concentration of unloaded free 5-ALA. The loading capacity of bPEI$_{25\,000}$-CDs was determined according to the difference between the total amount of 5-ALA and the unloaded 5-ALA outside the dialysis bag. For the loading capacity measurement, 1.0 mg of bPEI$_{25\,000}$-CDs and varying amounts of 5-ALA (with mass ratios of 2:1, 1:1, 1:3, and 1:5) were dissolved in 10 mL of a PBS buffer solution (0.01 mol/L, pH 7.4). Then, the mixture was stirred in the dark at 5 °C for 4 h and further dialyzed against 1500 mL of deionized water using a 0.5−1.0 kDa dialysis bag for 24 h to remove any unloaded 5-ALA. Finally, the free 5-ALA external dialysis bag was quantified according to the steps outlined in the calibration curve experiment (Text S3).

2.5. Preparation of Bacterial Suspension. *E. coli* was inoculated on nutrient agar and incubated at 37 °C for 24 h to obtain a single colony. Then, the colonies were selected by an inoculation ring and cultured in MHB medium for 12 h (37 °C, 200 rpm/min). Finally, the concentration of the bacterial suspension was adjusted to 10^8 CFU/mL by measuring the absorbance at 600 nm.

2.6. Antibacterial Activity Evaluation. The antibacterial activity was evaluated using the broth microdilution method and plate count method under different environmental stimuli (in the dark or in the light). The control groups were bacterial suspensions in 100 μL of MHB medium. In the broth microdilution method, 50 μL of bacterial suspension was seeded in 96-well plates at a concentration of 1.5 × 10^6 CFU/mL followed by the addition of 50 μL different concentrations of bacteriostats. In the dark group, the absorbance of each well at 600 nm was measured after 20 h of incubation in the dark, and the lowest concentration of bacteria-free well observed by the naked eye was determined as the minimum inhibitory concentration (MIC). In the light group, all samples were irradiated with a 633 nm laser after being treated with drugs in the dark for 4 h and then incubated in the dark until measured. In the plate count method, 10^6 CFU/mL of bacterial suspensions cultured with different bacteriostats were used as drug-treated samples. After 4 h of incubation, samples in the dark and light groups were diluted to appropriate concentrations and smeared on a nutrient agar plate. The colony numbers on each plate were counted after culturing for 24 h of culturing.

2.7. Other Characterizations. Detailed information on the hemolysis test, cytotoxicity test, membrane potential measurement, intracellular ROS detection, and bacterial morphological characterization are provided in Text S4−S8, respectively.

3. RESULTS AND DISCUSSION

3.1. Preparation and Optimization of bPEI$_{25\,000}$-CDs. It is widely acknowledged that both antibacterial efficacy and biosafety are crucial factors in the application of nanomedication. Therefore, bPEI$_{25\,000}$-CDs with optimized performance were first prepared. We synthesized five bPEI$_{25\,000}$-CDs using 0.7 g of citric acid monohydrate and varying amounts of bPEI$_{25\,000}$ (0.52, 1.05, 2.10, 4.20, and 6.30 g), which were sequentially labeled as 1−5. We then evaluated their antibacterial efficacy and biosafety properties. Figure 2a shows the proliferation curves of *E. coli* after 20 h of incubation with different bPEI$_{25\,000}$-CDs, which clearly reveals that the increase of the bPEI$_{25\,000}$ precursor significantly enhances the antibacterial ability of bPEI$_{25\,000}$-CDs. The MIC values of both bPEI$_{25\,000}$-CDs$_1$ and bPEI$_{25\,000}$-CDs$_2$ were above 2.5 mg/mL, while the MIC values of bPEI$_{25\,000}$-CDs$_3$, bPEI$_{25\,000}$-CDs$_4$, and

https://doi.org/10.1021/acsomega.3c08914
ACS Omega 2024, 9, 7034−7042

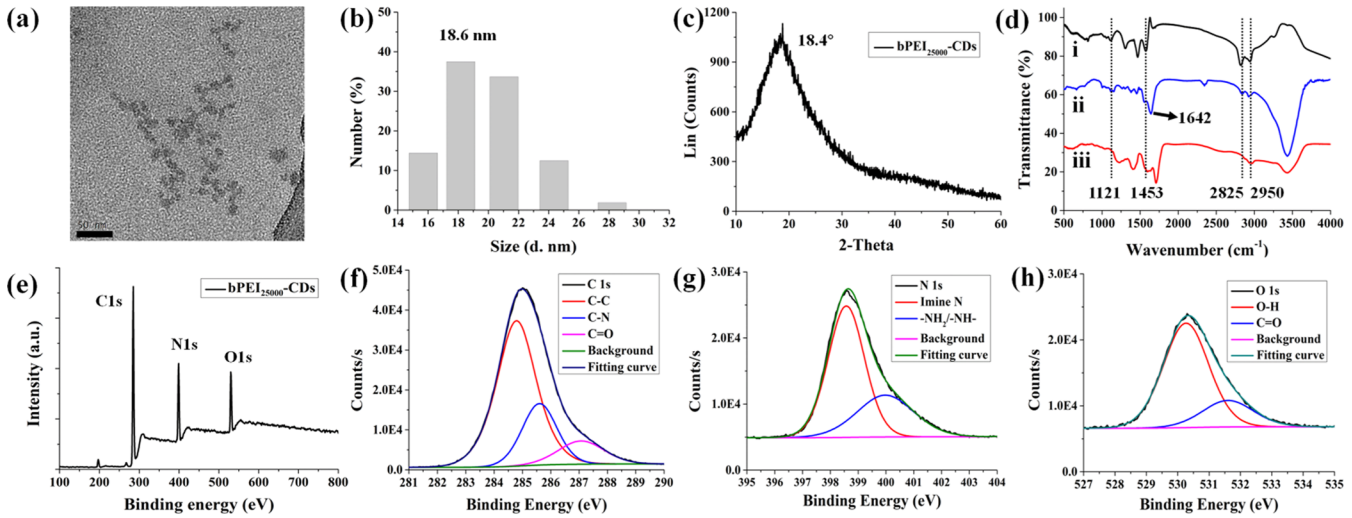

Figure 3. Characterization of the optimized bPEI$_{25\,000}$-CDs. (a) The morphology image of bPEI$_{25\,000}$-CDs with a scale bar of 50 nm. (b) The size distribution investigation by DLS measurement. (c) XRD analysis. (d) FITR image ((i) bPEI$_{25\,000}$, (ii) bPEI$_{25\,000}$-CDs, and (iii) bare CDs). (e) XPS survey scan of bPEI$_{25\,000}$-CDs. (f) High-resolution survey scan of the C 1s region, (g) N 1s region, and (h) O 1s region.

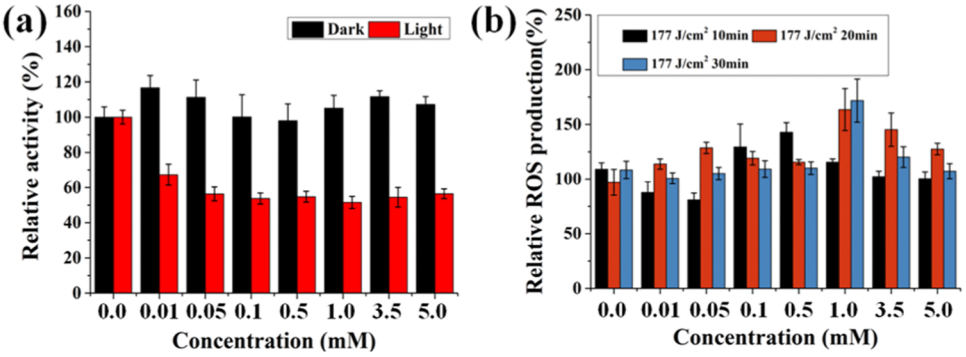

Figure 4. (a) Growth activity of *E. coli* treated with different concentrations of 5-ALA in the dark and in the light (the irradiation parameters were set at 148 mW/cm^2, 20 min, and 177 J/cm^2). (b) Determination of the relative ROS production in *E. coli* after incubation with 5-ALA under different irradiation conditions.

bPEI$_{25\,000}$-CDs$_5$ were 2.5, 1.0, and 0.75 mg/mL, respectively. We further evaluated their blood compatibility by calculating the hemolysis rate (Table S1). The results showed that bPEI$_{25\,000}$-CDs$_5$ fails to meet the requirements of less than 5.0% in the International Organization for the Hemolysis Rate Test (ISO number: 10933-4) even at a relatively low concentration (0.125 mg/mL). Conversely, bPEI$_{25\,000}$-CDs$_3$ and bPEI$_{25\,000}$-CDs$_4$ exhibited satisfactory antibacterial properties and qualified hemolysis rates, indicating their potentials for biomedical applications (Figure 2b). Subsequently, the cytotoxicities of bPEI$_{25\,000}$-CDs$_3$ and bPEI$_{25\,000}$-CDs$_4$ on L02, HEK-293T, and HSF cells were determined to assess their health risks to human exposure during clinical use, including hepatic metabolism, renal metabolism, and skin contact. It was shown that even at the highest concentration of 4.0 mg/mL, the relative cell viability of L02, HEK-293T, and HSF remained above 80% after incubation with bPEI$_{25\,000}$-CDs$_3$ (Figure 2c–2e, respectively). However, the relative cell viabilities of the bPEI$_{25\,000}$-CDs$_4$-treated group were only 9.06, 32.41, and 4.60% for L02, HEK-293T, and HSF cells at its MIC (1.0 mg/mL), respectively. Consequently, bPEI$_{25\,000}$-CDs$_3$ is verified as the preferred candidate for clinical treatment, which is described as the optimized bPEI$_{25\,000}$-CDs in the following experiments.

3.2. Characterization of the Optimized bPEI$_{25\,000}$-CDs.

The morphology and structure of the optimized bPEI$_{25\,000}$-CDs were further explored (Figure 3a,b). The morphology image of the optimized bPEI$_{25\,000}$-CDs depicted nearly spherical carbon particles, and the hydration radius of the optimized bPEI$_{25\,000}$-CDs ranged from 15.7 to 28.2 nm with the average diameter determined to be 18.6 nm (Figure 3b). In addition, a sharp distinction in surface charge between the bare CDs (−4.7 mV) and the optimized bPEI$_{25\,000}$-CDs (+13.1 mV) was detected, highlighting the crucial role of bPEI$_{25\,000}$ in endowing CDs with a positive surface potential (Table S2). Subsequently, the samples were analyzed by X-ray diffractometer (XRD), Fourier transform infrared spectroscopy (FTIR), and X-ray photoelectron spectroscopy (XPS) to obtain structural and functional group information. The XRD pattern revealed a broad and low-intensity diffraction peak centered at 18.4°, indicating an amorphous structure (Figure 3c). The characteristic peaks in the FTIR spectrum of bPEI$_{25\,000}$ (Figure 3d, line (i)) could also be found in the spectrum of the optimized bPEI$_{25\,000}$-CDs (Figure 3d, line (ii)). This was attributed to the stretching vibration of C−N groups at 1121 cm^{-1}, the in-plane bending, and the symmetric and asymmetric vibrations of CH_2 groups at 1453 cm^{-1}, 2825, and 2950 cm^{-1}, respectively. Meanwhile, the appearance of the

https://doi.org/10.1021/acsomega.3c08914
ACS Omega 2024, 9, 7034−7042

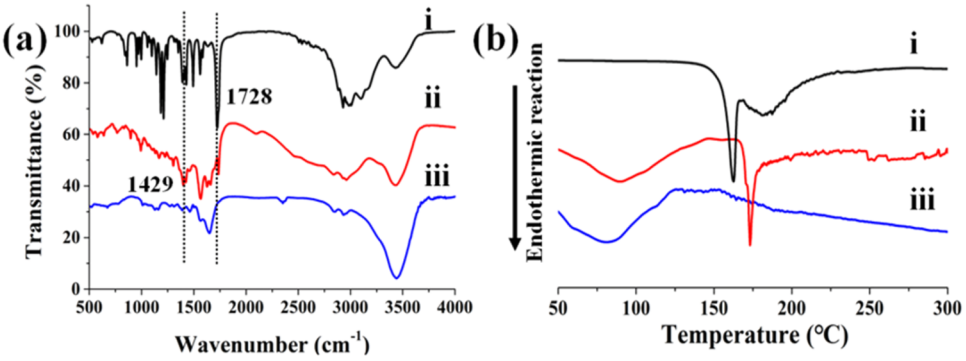

Figure 5. (a) FTIR spectra and (b) DSC measurement of the optimized $bPEI_{25\,000}$-CDs before and after combination with 1.0 mM 5-ALA ((i) 5-ALA, (ii) ALA-$bPEI_{25\,000}$-CDs, and (iii) $bPEI_{25\,000}$-CDs).

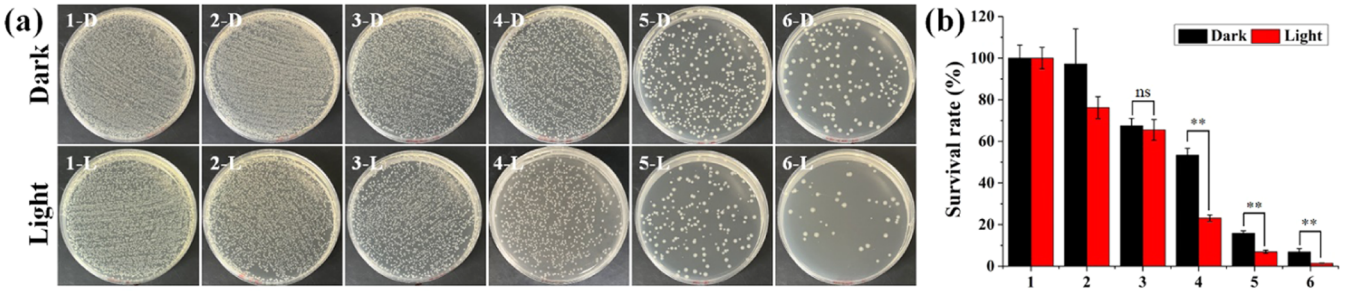

Figure 6. (a) The growth activity investigation of *E. coli* using plate count method and (b) the corresponding relative survival rate (groups 1−6 represent bacterial proliferation under different stimulation conditions: 1 is the control group; 2 is the 5-ALA-treated group at 1.0 mM; 3 and 4 are the $bPEI_{25\,000}$-CD-treated group and ALA-$bPEI_{25\,000}$-CD-treated group (with 0.5 × MIC of $bPEI_{25\,000}$-CDs as a carrier), respectively; 5 and 6 are the $bPEI_{25\,000}$-CD-treated group and ALA-$bPEI_{25\,000}$-CD-treated group (with 1.0 × MIC of $bPEI_{25\,000}$-CDs as a carrier), respectively). The laser irradiation was performed with a 633 nm laser (98 mW/cm^2, 30 min, 177 J/cm^2).

C═O stretching in the amide linkage at 1642 cm^{-1} indicated the presence of $bPEI_{25\,000}$ residues on the surface of the optimized $bPEI_{25\,000}$-CDs. The IR spectrum comparison between the bare CDs (Figure 3d, line (iii)) and the optimized $bPEI_{25\,000}$-CDs confirmed that citric acid had reacted with $bPEI_{25\,000}$ to yield $bPEI_{25\,000}$-CDs during hydrothermal treatment. Furthermore, the element identification of the optimized $bPEI_{25\,000}$-CDs showed three peaks, representing 74.72% of carbon, 13.09% of nitrogen, and 12.19% of oxygen (Figure 3e). The high-resolution survey scan of C 1s in $bPEI_{25\,000}$-CDs demonstrated the existence of C−C at 284.8 eV, C−N at 285.6 eV, and C═O group at 287.1 eV (Figure 3f), while that of N 1s in Figure 3g indicated the formation of imine N and -NH_2 /-NH at 398.6 and 400.0 eV, respectively. Meanwhile, peaks at 530.3 and 531.6 eV in Figure 3h confirmed the existence of the −OH and C═O bonds. Therefore, we have provided convincing evidence for the successful fabrication of $bPEI_{25\,000}$-CDs that possess both biosafety and antibacterial properties after optimization.

3.3. Evaluation of the 5-ALA-Induced PDT Effect on *E. coli*. As one of the commonly used photodynamic agents, 5-ALA has gradually drawn attention for its antibacterial application. Since the elimination ability of 5-ALA is affected by several factors, including concentration, irradiation intensity, and bacterial strains, prior to commencing the study, we preliminarily optimized the treatment parameters of 5-ALA-induced PDT therapy for *E. coli*. Figure 4a shows that different doses of 5-ALA had no significant measurable effect on the growth activity of *E. coli* in the dark, indicating its relatively low dark toxicity at high concentrations up to 5.0 mM. After illumination (148 mW/cm^2, 20 min, 177 J/cm^2), the proliferation of *E. coli* showed a certain extent of a downward trend, suggesting that the effect of 5-ALA-induced PDT on the growth activity of *E. coli* was limited.

In addition to the concentration, previous reports have also indicated that the PDT effect mediated by 5-ALA is closely related to irradiation dosage and a high light dose may enable 5-ALA to achieve an excellent sterilization effect against bacteria at relatively low concentration. However, a higher energy is not always optimal in clinical practice because it is necessary to protect normal cells from PDT damage, and the perception of patients should also be considered. Therefore, an effective and safe laser dose for PDT treatment should be less than 192 J/cm^2 in most cases.[34] Thus, the optimal loading dose of 5-ALA was determined by detecting the generated ROS in *E. coli* with different irradiation durations (10, 20, and 30 min) under a total dose of 177 J/cm^2. Figure 4b depicts that after 10 min of irradiation (296 mW/cm^2), the intracellular ROS increased by a maximum of 42.5% under the stimulation of 0.5 mM 5-ALA. When the irradiation time was extended to 20 min (148 mW/cm^2) and 30 min (98 mW/cm^2), the ROS production reached a peak with the administration of 1.0 mM 5-ALA, increasing by 63.6 and 71.8%, respectively. Hence, the optimal loading dose of 5-ALA was determined to be 1.0 mM, and the irradiation parameters were set at 98 mW/cm^2 for 30 min.

3.4. Characterization of ALA-$bPEI_{25\,000}$-CDs. The multidrug system was constructed by combining optimized $bPEI_{25\,000}$-CDs and 5-ALA (1.0 mM) through electrostatic interactions. The resulting nanocomposite was investigated by FTIR, differential scanning calorimetry (DSC), and zeta potential analysis. In this study, the loading capacity of the

https://doi.org/10.1021/acsomega.3c08914
ACS Omega 2024, 9, 7034−7042

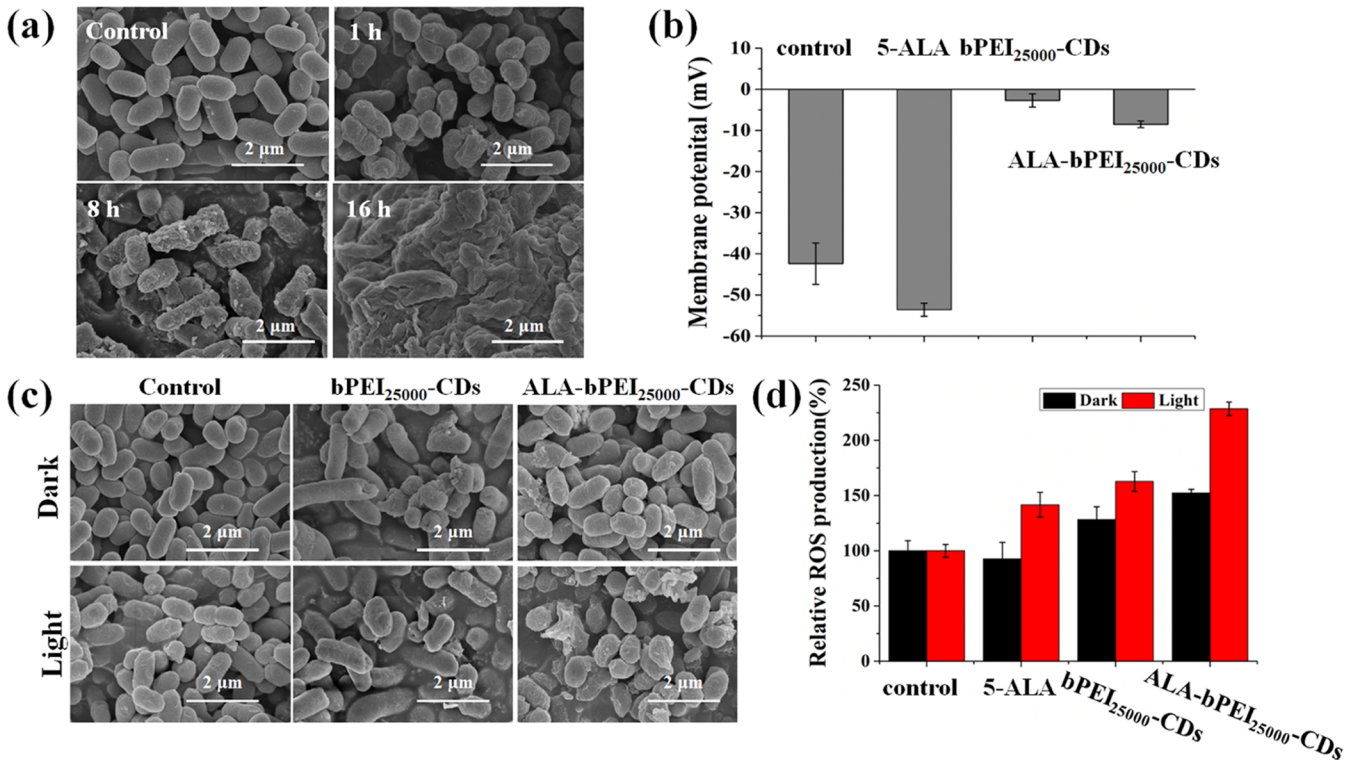

Figure 7. (a) The morphology characterization of *E. coli* treated with bPEI$_{25\,000}$-CDs in the dark for 1, 8, and 16 h. (b) The surface potential of *E. coli* treated with different stimulants for 1 h in the dark. (c) The morphology of *E. coli* under bPEI$_{25\,000}$-CD and ALA-bPEI$_{25\,000}$-CD stimulations in the dark and light after 1 h of incubation. (d) The intracellular ROS generation in *E. coli* treated with different stimulants in the dark and light.

optimized bPEI$_{25\,000}$-CDs for 5-ALA was quantified using the standard curve as aforementioned (Text S3 and Figure S1). It was suggested that 1.0 mg/mL of bPEI$_{25\,000}$-CDs was able to load up to 2.62 mg/mL of 5-ALA (15.6 mM) at pH 7.5, which is sufficient to meet the requirements for optimal ALA loading. Figure 5a shows the FTIR spectrum variation of bPEI$_{25\,000}$-CDs before and after integration with 5-ALA. Compared with bPEI$_{25\,000}$-CDs (Figure 5a, line (iii)), the characteristic peaks of 5-ALA (Figure 5a, line (i)) at 1728 and 1429 cm^{-1} and the peaks at 500−1000 cm^{-1} in the fingerprint region could also be found in the ALA-bPEI$_{25\,000}$-CD spectrum (Figure 5a, line (ii)), indicating the presence of 5-ALA for ALA-bPEI$_{25\,000}$-CDs after purification. The thermodynamic study by DSC revealed that the endothermic peak of 5-ALA at 162.7 °C (Figure 5b, line (i)) was absent for the bEI$_{25000}$-CD sample (Figure 5b, line (iii)), while an obvious melting point at a relatively high temperature of 172.9 °C appeared for ALA-bPEI$_{25\,000}$-CDs (Figure 5b, line (ii)), indicating the presence of 5-ALA. Therefore, the increase of the melting point temperature is probably due to the electrostatic forces between 5-ALA and bPEI$_{25\,000}$-CDs.

3.5. Bacterial Inactivation Study of ALA-bPEI$_{25\,000}$-CDs. The bacterial inactivation ability of ALA-bPEI$_{25\,000}$-CDs was evaluated using the plate count method (Figure 6a), and the corresponding bacterial survival rate is illustrated in Figure 6b. Figure 6a depicts that the proliferation of *E. coli* in the dark control group (1-D) was similar to that in the light control group (1-L), indicating that the laser irradiation used in this study rarely affects the growth of *E. coli*. As expected, 1.0 mM 5-ALA showed negligible dark toxicity and limited phototoxicity (76.2% of cell viability after irradiation) against *E. coli* (2-D and 2-L). In the bPEI$_{25\,000}$-CD-treated group, the bacterial survival rate after photoexcitation declined from 67.5 to 65.5% at s dose of 0.5 × MIC for the optimized bPEI$_{25\,000}$-CDs (1.25 mg/mL in 3-D and 3-L, $p > 0.05$), while the survival rate changed from 15.8% to 6.9% at a dose of 1.0 × MIC (2.5 mg/mL in 5-D and 5-L, $p < 0.01$), demonstrating that bPEI$_{25\,000}$-CDs also have concentration-dependent phototoxicity to *E. coli*. In addition, ALA-bPEI$_{25\,000}$-CDs presented enhanced antibacterial efficacy when applied to *E. coli*. In Figure 6, panels 6-D and 6-L illustrate the growth activity of *E. coli* stimulated by ALA-bPEI$_{25\,000}$-CDs at 0.5 × MIC in the dark and light, respectively, which can be seen that a marked decrease in survival rate was observed and the elimination efficiency has increased by 30.2% due to the PDT effect induced by ALA-bPEI$_{25\,000}$-CDs. Meanwhile, increasing the concentration of ALA-bPEI$_{25\,000}$-CDs to 1.0 × MIC resulted in a strong decrease in the activity rate from 6.8% to 1.5% (6-D and 6-L, $p < 0.01$). What emerges from the results reported here is that a highly efficient killing ability of ALA-bPEI$_{25\,000}$-CDs against *E. coli* was achieved, which was clearly enhanced compared to using them solely.

3.6. Exploration of Possible Mechanisms. To explore the possible mechanisms, the morphological properties of the *E. coli* samples treated with the optimized bPEI$_{25\,000}$-CDs were first investigated with SEM study (Figure 7a). With the extension of incubation time, the *E. coli* cells presented rough surfaces and deformed morphology, eventually leading to a complete cell fragmentation after 16 h of incubation, which confirmed the disruptive effect of the optimized bPEI$_{25\,000}$-CDs on cell membrane integrity. These results are consistent with previous research, which has noted the importance of the electrostatic action of the positively charged PEI or PEI-functionalized particles on the high interaction with bacterial

https://doi.org/10.1021/acsomega.3c08914
ACS Omega 2024, 9, 7034−7042

membranes, which can lead to membrane disruption and leakage of cell contents.[38,39] Subsequently, the membrane potential study of *E. coli* treated with various stimulants was conducted to investigate the binding condition of ALA-bPEI$_{25\,000}$-CDs to cell membranes. Figure 7b and Table S3 demonstrate that the surface potential of bPEI$_{25\,000}$-CDs was +13.1 mV, which decreased to +4.2 mV after being assembled with 5-ALA, indicating that the positively charged surface characteristics are kept for ALA-bPEI$_{25\,000}$-CDs. Meanwhile, the membrane potential was −42.4 mV for untreated *E. coli* but slightly dropped to −53.6 mV for 5-ALA-incubated *E. coli*. In contrast, the zeta potential increased dramatically to −2.7 mV and −8.5 mV for *E. coli* samples incubated with bPEI$_{25\,000}$-CDs and ALA-bPEI$_{25\,000}$-CDs, respectively, demonstrating a strong interaction effect. The influence of photoexcitation on the morphological properties of *E. coli* with different treatments for 1 h was also explored. As shown in Figure 7c, the cell envelope in the control group was smooth and intact in both the dark and light groups, which was consistent with the result using the plate count method, indicating that laser irradiation had no apparent impact on the *E. coli* growth. In the bPEI$_{25\,000}$-CD-treated group, bacterial morphology presented an irregular shape and a sunken tip region in the dark and became sharply irregular and less well-defined after irradiation. In the ALA-bPEI$_{25\,000}$-CD-treated group, damaged and even fragmented cells could also be captured in the dark group, which became more serious after laser irradiation. The phenomenon observed in the dark was consistent with the results shown in Figure 7a,b, indicating that the positively charged bPEI$_{25\,000}$-CDs and ALA-bPEI$_{25\,000}$-CDs could induce cell damage even in the dark. However, changes in cell morphology were also studied with intracellular ROS generation measurements (Figure 7d and Table S4). It showed that only *E. coli* incubated with bPEI$_{25\,000}$-CDs and ALA-bPEI$_{25\,000}$-CDs in the dark exhibited a slight increase in the relative intracellular ROS generation, which could be attributed to the membrane dysfunction induced by the positively charged surfaces and the intrinsic ROS production by the damaged bacteria themselves in the form of "oxidative shielding" response.[39,40] On the contrary, an upward trend was detected after photoexcitation in all drug-stimulated groups. The highest relative ROS production was obtained for samples treated with ALA-bPEI$_{25\,000}$-CDs (2.28-fold). Taken together, the significantly enhanced antibacterial effect of ALA-bPEI$_{25\,000}$-CDs against *E. coli* may be partly attributed to the strong binding interaction of the cationic CDs with cell membranes, resulting in a disruption effect. Additionally, the combination of bPEI$_{25\,000}$-CDs with 5-ALA facilitates its approach to bacterial surfaces and their intake by cells, thereby introducing a more efficient PDT effect after irradiation.

4. CONCLUSIONS

In summary, this study reports an improvement in the antibacterial activity of cationic CD-based nanomedications against *E. coli* by assembling with 5-ALA, a commonly used hydrophilic molecule in photodynamic therapy. The cationic CDs (bPEI$_{25\,000}$-CDs) were synthesized through hydrothermal treatment of branched polyethylenimine (average MW 25000, bPEI$_{25\,000}$) and citric acid. They were initially optimized for high antibacterial property while ensuring a qualified biosafety. The ALA-bPEI$_{25\,000}$-CD was further fabricated by integrating bPEI$_{25\,000}$-CDs with 5-ALA via the electrostatic interaction, which exhibited significantly enhanced inhibitory ability against *E. coli* compared to those of 5-ALA and bPEI$_{25\,000}$-CDs. When the dose of bPEI$_{25\,000}$-CDs was reduced to half of the MIC, ALA-bPEI$_{25\,000}$-CDs still achieved a bacterial inhibition rate of over 70% after irradiation. Furthermore, the reason for the heightened antibacterial capacity of ALA-bPEI$_{25\,000}$-CDs was by means of bacterial morphology, membrane potential, and intracellular ROS production study, which implied that ALA-bPEI$_{25\,000}$-CD can take advantage of the high affinity of cationic CDs for cell membranes to disrupt their integrity and cause cellular damage. Meanwhile, it may promote the permeation of 5-ALA, resulting in a substantial increase in intracellular ROS after light exposure. This work provides novel approaches to expand the use of CD-based antibacterial applications, and further studies are required to fully comprehend the antibacterial mechanism and the antibacterial activity against various bacterial strains.

■ ASSOCIATED CONTENT

Supporting Information

The Supporting Information is available free of charge at https://pubs.acs.org/doi/10.1021/acsomega.3c08914.

Materials; instrumentation and measurements; the calibration curve of unloaded 5-ALA; hemolysis test; cytotoxicity test; membrane potential characterization; intracellular ROS detection; bacterial morphological characterization; hemolysis rate of different bPEI$_{25\,000}$-CDs; the zeta potential characterization of the optimized bPEI$_{25\,000}$-CDs and bare CDs; the standard curve for detection of free 5-ALA; the membrane potential of *E. coli* treated with different stimulants; and measurement of the relative intracellular ROS generation (PDF)

■ AUTHOR INFORMATION

Corresponding Authors

Jingfang Shangguan − *School of Pharmacy, Xinxiang Medical University, Xinxiang, Henan 453003, China;* orcid.org/0000-0002-7781-7938; Email: sgjf1988@126.com

Wei Liu − *School of Pharmacy, Xinxiang Medical University, Xinxiang, Henan 453003, China;* orcid.org/0000-0002-3830-6692; Email: liuwei@xxmu.edu.cn

Authors

Zhenjing Wu − *School of Pharmacy, Xinxiang Medical University, Xinxiang, Henan 453003, China*

Chengjie Qiao − *School of Pharmacy, Xinxiang Medical University, Xinxiang, Henan 453003, China*

Yuyang Zhang − *School of Pharmacy, Xinxiang Medical University, Xinxiang, Henan 453003, China*

Lin Li − *School of Pharmacy, Xinxiang Medical University, Xinxiang, Henan 453003, China*

Qilu Li − *Key Laboratory for Yellow River and Huai River Water Environment and Pollution Control, Ministry of Education, School of Environment, Henan Normal University, Xinxiang, Henan 453007, China;* orcid.org/0000-0003-0442-353X

Yiqiao Gao − *School of Pharmacy, Xinxiang Medical University, Xinxiang, Henan 453003, China*

Huijuan Yan − *School of Pharmacy, Xinxiang Medical University, Xinxiang, Henan 453003, China*

Complete contact information is available at: https://pubs.acs.org/10.1021/acsomega.3c08914

https://doi.org/10.1021/acsomega.3c08914
ACS Omega 2024, 9, 7034−7042

Author Contributions

J.S. contributed to the experimental design, funding acquisition, project administration, and manuscript composition. Z.W. and C.Q. contributed to methodology, validation, and investigation. Y.Z. and L.L. contributed to formal analysis and cured the data. Q.L. contributed to resources, methodology, and formal analysis. Y.G. and H.Y. contributed to resources and writing—review and editing. W.L. contributed to project administration and funding acquisition.

Notes

The authors declare no competing financial interest.

■ ACKNOWLEDGMENTS

This work was jointly supported by the National Natural Science Foundation of China (grant number 21804116), the Henan Provincial Science and Technology Research Project (grant numbers 232102231029, 222102310411), and the Doctorial Starting Fund of Xinxiang Medical University (grant number XYBSKYZZ201807).

■ REFERENCES

(1) 2020 Antibacterial agents in clinical and preclinical development: an overview and analysis. Geneva: WHO, 2021, ISBN 978-92-4-002130-3. http://www.who.int/publications/i/item/9789240021303.
(2) Chen, S.; Quan, Y.; Yu, Y. L.; Wang, J. H. Graphene quantum dot/silver nanoparticle hybrids with oxidase activities for antibacterial application. *ACS Biomater. Sci. Eng.* **2017**, 3 (3), 313−321.
(3) Ghosh, P.; Bairagi, D.; Hazra, N.; Jana, S.; Banerjee, A. Carbon-dot-decorated silver and gold nanocomposites for antibacterial activity and degradation of organic dyes. *ACS Appl. Nano Mater.* **2023**, *6*, 18100−18112.
(4) Phuinthiang, P.; Trinh, D. T. T.; Channei, D.; Ratananikom, K.; Sirilak, S.; Khanitchaidecha, W.; Nakaruk, A. Novel strategy for the development of antibacterial TiO_2 thin film onto polymer substrate at room temperature. *Nanomaterials* **2021**, *11* (6), 1493.
(5) Padmanabhan, N. T.; Thomas, R. M.; John, H. Antibacterial self-cleaning binary and ternary hybrid photocatalysts of titanium dioxide with silver and graphene. *J. Environ. Chem. Eng.* **2022**, *10*, No. 107275.
(6) Wang, F.; Tan, J.; Zhang, S.; Zhou, Y.; He, D.; Deng, L. Efficient eradication of bacterial biofilms with highly specific graphene-based nanocomposite sheets. *ACS Biomater. Sci. Eng.* **2021**, 7 (11), 5118−5128.
(7) Perreault, F.; Faria, A. F.; Nejati, S.; Elimelech, M. Antimicrobial properties of graphene oxide nanosheets: why size matters. *ACS Nano* **2015**, *9* (7), 7226−7236.
(8) Kuroki, A.; Tchoupa, A. K.; Hartlieb, M.; Peltier, R.; Locock, K. E. S.; Unnikrishnan, M.; Perrier, S. Targeting intracellular, multi-drug resistant *Staphylococcus aureus* with guanidinium polymers by elucidating the structure-activity relationship. *Biomaterials* **2019**, *217*, No. 119249.
(9) Vimbela, G. V.; Ngo, S. M.; Fraze, C.; Yang, L.; Stout, D. A. Antibacterial properties and toxicity from metallic nanomaterials. *Int. J. Nanomed.* **2017**, *Volume 12*, 3941−3965.
(10) Senut, M. C.; Zhang, Y.; Liu, F.; Sen, A.; Ruden, D. M.; Mao, G. Size-dependent toxicity of gold nanoparticles on human embryonic stem cells and their neural derivatives. *Small* **2016**, *12* (5), 631−646.
(11) Dubey, N.; Dhiman, S.; Koner, A. L. Review of carbon dot-based drug conjugates for cancer therapy. *ACS Appl. Nano Mater.* **2023**, *6*, 4078−4096.
(12) Bai, Y.; Wang, Y.; Cao, L.; et al. Self-targeting carbon quantum dots for peroxynitrite detection and imaging in live cells. *Anal. Chem.* **2021**, *93* (49), 16466−16473.
(13) Anand, S. R.; Bhati, A.; Saini, D.; Gunture; Chauhan, N.; Khare, P.; Sonkar, S. K. Antibacterial nitrogen-doped carbon dots as a reversible "fluorescent nanoswitch" and fluorescent ink. *ACS Omega* **2019**, *4*, 1581−1591.
(14) Jiang, Y.; Zhao, X.; Zhou, X.; et al. Multifunctional carbon nanodots for antibacterial enhancement, pH change, and poisonous Tin (IV) specifical detection. *ACS Omega* **2023**, *8*, 41469−41479.
(15) Geng, X.; Sun, Y.; Guo, Y.; et al. Fluorescent carbon dots for in situ monitoring of lysosomal ATP levels. *Anal. Chem.* **2020**, *92* (11), 7940−7946.
(16) Wang, J.; Zheng, J.; Yang, Y.; Liu, X.; Qiu, J.; Tian, Y. Tunable full-color solid-state fluorescent carbon dots for light emitting diodes. *Carbon* **2022**, *190*, 22−31.
(17) Achilleos, D. S.; Yang, W.; Kasap, H.; Savateev, A.; Markushyna, Y.; Durrant, J. R.; Reisner, E. Solar reforming of biomass with homogeneous carbon dots. *Angew. Chem. Int. Ed.* **2020**, *59* (41), 18184−18188.
(18) Cailotto, S.; Massari, D.; Gigli, M.; et al. N-doped carbon dot hydrogels from brewing waste for photocatalytic wastewater treatment. *ACS Omega* **2022**, *7*, 4052−4061.
(19) Zhang, M.; Wang, W.; Wu, F.; et al. Biodegradable poly(γ-glutamic acid)@glucose oxidase@carbon dot nanoparticles for simultaneous multimodal imaging and synergetic cancer therapy. *Biomaterials* **2020**, *252*, No. 120106.
(20) Dada, S. N.; Babanyinah, G. K.; Tetteh, M. T.; et al. Covalent and noncovalent loading of doxorubicin by folic acid-carbon dot nanoparticles for cancer theranostics. *ACS Omega* **2022**, *7*, 23322−23331.
(21) Chen, Z.; Lv, Z.; Sun, Y.; Chi, Z.; Qing, G. Recent advancements in polyethyleneimine-based materials and their biomedical, biotechnology, and biomaterial applications. *J. Mater. Chem. B* **2020**, *8* (15), 2951−2973.
(22) Li, R.; Wei, F.; Wu, X.; et al. PEI modified orange emissive carbon dots with excitation-independent fluorescence emission for cellular imaging and siRNA delivery. *Carbon* **2021**, *177*, 403−411.
(23) Azevedo, M. M.; Ramalho, P.; Silva, A. P.; Teixeira-Santos, R.; Pina-Vaz, C.; Rodrigues, A. G. Polyethyleneimine and polyethyleneimine-based nanoparticles: novel bacterial and yeast biofilm inhibitors. *J. Med. Microbiol.* **2014**, *63*, 1167−1173.
(24) Zhao, D.; Liu, X.; Zhang, R.; Xiao, X.; Li, J. Preparation of two types of silver-doped fluorescent carbon dots and determination of their antibacterial properties. *J. Inorg. Biochem.* **2021**, *214*, No. 111306.
(25) Abu Rabe, D. I.; Al Awak, M. M.; Yang, F.; et al. The dominant role of surface functionalization in carbon dots' photo-activated antibacterial activity. *Int. J. Nanomed.* **2019**, *14*, 2655−2665.
(26) Liu, M.; Guo, R.; Ma, Y. Construction of a specific and efficient antibacterial agent against *Pseudomonas aeruginosa* based on polyethyleneimine cross-linked fucose. *J. Mater. Sci.* **2021**, *56* (10), 6083−6094.
(27) Zhao, C.; Wu, L.; Wang, X. Quaternary ammonium modified carbon quantum dots as an antimicrobial agent against gram-positive bacteria for the treatment of MRSA-infected pneumonia in mice. *Carbon* **2020**, *163*, 70−84.
(28) Liu, M.; Li, J.; Li, B. Mannose-modificated polyethylenimine: a specific and effective antibacterial agent against *Escherichia coli*. *Langmuir* **2018**, *34*, 1574−1580.
(29) Li, S.; Guo, Z.; Zhang, Y.; Xue, W.; Liu, Z. Blood compatibility evaluations of fluorescent carbon dots. *ACS Appl. Mater. Interfaces* **2015**, *7*, 19153−19162.
(30) Tewari, K. M.; Dondi, R.; Yaghini, E.; Pourzand, C.; MacRobert, A. J.; Eggleston, I. M. Peptide-targeted dendrimeric prodrugs of 5-aminolevulinic acid: a novel approach towards enhanced accumulation of protoporphyrin IX for photodynamic therapy. *Bioorg. Chem.* **2021**, *109*, No. 104667.
(31) Chen, Y.; Zhang, Z.; Xin, Y.; et al. Functional transdermal nanoethosomes enhance photodynamic therapy of hypertrophic scars *via* self-generating oxygen. *ACS Appl. Mater. Interfaces* **2021**, *13* (7), 7955−7965.
(32) You, C.; Ning, L.; Wu, H.; Huang, C.; Wang, F. A biocompatible and pH-responsive nanohydrogel based on cellulose nanocrystal for enhanced toxic reactive oxygen species generation. *Carbohydr. Polym.* **2021**, *258*, No. 117685.

https://doi.org/10.1021/acsomega.3c08914
ACS Omega 2024, 9, 7034−7042

(33) Hsieh, C. M.; Huang, Y. H.; Chen, C. P.; Hsieh, B. C.; Tsai, T. 5-Aminolevulinic Acid Induced Photodynamic Inactivation on *Staphylococcus aureus* and *Pseudomonas aeruginosa*. *J. Food Drug Anal.* **2014**, *22* (3), 350−355.
(34) Huang, J.; Guo, M.; Jin, S.; et al. Antibacterial photodynamic therapy mediated by 5-aminolevulinic acid on methicillin-resistant *Staphylococcus aureus*. *Photodiagn. Photodyn. Ther.* **2019**, *28*, 330−337.
(35) Nitzan, Y.; Salmon-Divon, M.; Shporen, E.; Malik, Z. ALA induced photodynamic effects on gram positive and negative bacteria. *Photochem. Photobiol. Sci.* **2004**, *3* (5), 430−435.
(36) Fotinos, N.; Convert, M.; Piffaretti, J. C.; Gurny, R.; Lange, N. Effects on gram-negative and gram-positive bacteria mediated by 5-aminolevulinic acid and 5-aminolevulinic acid derivatives. *Antimicrob. Agents Chemother.* **2008**, *52* (4), 1366−1373.
(37) Bohm, G. C.; Gándara, L.; Venosa, G. D.; Mamone, L.; Buzzola, F.; Casas, A. Photodynamic inactivation mediated by 5-aminolevulinic acid of bacteria in planktonic and biofilm forms. *Biochem. Pharmacol.* **2020**, *177*, No. 114016.
(38) Wiegand, C.; Bauerb, M.; Hipler, U. C.; Fischer, D. Poly(ethyleneimines) in dermal applications: biocompatibility and antimicrobial effects. *Int. J. Pharm.* **2013**, *456*, 65−174.
(39) Bing, W.; Sun, H.; Yan, Z.; Ren, J.; Qu, X. Programmed bacteria death induced by carbon dots with different surface charge. *Small* **2016**, *12*, 4713−4718.
(40) Ristic, B. Z.; Milenkovic, M. M.; Dakic, I. R.; et al. Photodynamic antibacterial effect of graphene quantum dots. *Biomaterials* **2014**, *35*, No. 4428.

https://doi.org/10.1021/acsomega.3c08914
ACS Omega 2024, 9, 7034−7042